Thermal transformation of cubic-shaped MSn(OH)_6 (M = Ca, Mn, Co, and Zn) hydroxides to SnO_2-MO_x mixed oxides

Yamaura, Hiroyuki
Department of Materials Science and Biotechnology, Graduate School of Science and Engineering, Ehime University

Tajima, Emiri
Department of Materials Science and Biotechnology, Graduate School of Science and Engineering, Ehime University

Nishibori, Maiko
Department of Advanced Materials Science and Engineering, Faculty of Engineering Sciences, Kyushu University

Yamaguchi, Syuhei
Department of Materials Science and Biotechnology, Graduate School of Science and Engineering, Ehime University

他

出版情報：Journal of the Ceramic Society of Japan. 130 (8), pp.715-722, 2022-08-01. Ceramic Society of Japan
バージョン：

Journal of the Ceramic Society of Japan 130 [8] 715-722 2022
DOI http://doi.org/10.2109/jcersj2.21170

JCS-Japan

FULL PAPER

Thermal transformation of cubic-shaped $MSn(OH)_6$ (M = Ca, Mn, Co, and Zn) hydroxides to SnO_2–MO_x mixed oxides

Hiroyuki Yamaura[1,†], Emiri Tajima[1], Maiko Nishibori[2], Syuhei Yamaguchi[1], Kengo Shimanoe[2] and Hidenori Yahiro[1]

[1] Department of Materials Science and Biotechnology, Graduate School of Science and Engineering, Ehime University, Matsuyama 790–8577, Japan
[2] Department of Advanced Materials Science and Engineering, Faculty of Engineering Sciences, Kyushu University, 6–1 Kasuga-koen, Kasuga, Fukuoka 816–8580, Japan

The tin–metal mixed hydroxides $CaSn(OH)_6$, $MnSn(OH)_6$, $CoSn(OH)_6$, and $ZnSn(OH)_6$, with cubic morphologies, were prepared using a coprecipitation method; they were subsequently transformed into the corresponding tin–metal mixed oxides by calcination at 600–900 °C. The crystalline structures and the morphologies of the various samples at each calcination step (just prepared, dried at 110 °C, and calcined at 600 and 900 °C) were systematically evaluated by X-ray diffractometry, scanning electron microscopy, transmission electron microscopy, and X-ray absorption fine structure analyses. The cubic shapes of the $CaSn(OH)_6$ and $ZnSn(OH)_6$ nanoparticles were maintained after calcination of them at 600 and 900 °C, while those of $MnSn(OH)_6$ and $CoSn(OH)_6$ ones were not maintained after calcination of them.

Key-words : Tin dioxide, Cubic, Hydroxystannate, Nanoparticles, Composite oxide

[Received December 6, 2021; Accepted May 31, 2022]

1. Introduction

Shape-controlled tin–metal mixed oxides have been attracting a great deal of attention due to their potential uses as catalysts,[1] photocatalysts,[2)–4] gas sensors,[5),6] and electrodes.[7)–9] Zn–Sn oxides have been reported to exhibit a range of morphologies, such as nanorod,[10] nanowire,[11] and polyhedron,[12] and the morphologies have been determined to largely depend on preparation conditions. $MSn(OH)_6$ (M = Ca, Mn, Co, and Zn) is a precursor used to prepare metal–tin mixed oxides; in the hydroxides, metal ions are octahedrally coordinated by O atoms; indeed, these species comprise $Sn(OH)_6$ and $M(OH)_6$ moieties that share the corner of the O atom.[13]

Controlling the shape of the particles of tin–metal mixed oxides is of significant interest from the standpoint of using these oxides as sensors and photocatalysts, as controlling the said characteristics may afford the emergence of new electrical and optical properties.[14),15] In particular, the formation of nanoparticles with mesoporous structure is attractive in the preparation of gas-sensing materials,[16] as the presence of such structural units may ensure a rapid gas response; however, maintaining the high surface area of nanoparticles is a difficult goal to achieve when gas sensors are used in high-temperature operations. In this context, the formation of hierarchical nanostructures is expected to afford the development of high-potential materials that do not undergo particle agglomeration.

A number of studies have been published that focused on gas sensors composed of cubic tin–metal oxides. For example, Ma et al. prepared $ZnSnO_3$, which comprised cubic hollow structures and was used as a H_2S gas sensor.[17] Cao et al. prepared $ZnSnO_3$ nanocubes that were used as ethanol gas sensors.[18] Huang et al. obtained hollow porous SnO_2 microcubes via thermal decomposition of the relevant precursors [$CoSn(OH_6)$ and $MnSn(OH)_6$] followed by an acid-washing process; these microcubes were then used as sensors of volatile organic compounds.[19),20] The mixed oxides prepared in these studies all exhibited improved sensing performance. However, little is known about the details of the transformation of the precursor into the oxide as a result of heat treatment. In the present study, tin–metal mixed hydroxides were prepared by a simple coprecipitation method and successfully employed as precursors of tin–metal mixed oxides.[21] Furthermore, the mixed hydroxides prepared by coprecipitation were calcined at 250–900 °C to yield tin–metal mixed oxides. The influence of added metal ion (M = Ca, Mn, Co, and Zn) was investigated on transformation process of $MSn(OH)_6$ precursor to tin–metal mixed oxide with cubic shape and the change in its morphology by thermal treatment at 600–900 °C.

† Corresponding author: H. Yamaura; E-mail: yamaura.hiroyuki.mf@ehime-u.ac.jp

Table 1. Applied conditions for the preparation of tin–metal hydroxides

Sample	Sn conc. /mol·L^{-1}	M (Ca, Mn, Co, or Zn) conc. /mol·L^{-1}	Base	Stirring	
				Time/h	Temp./°C
Sn–Ca	0.1	0.1	NaOH	1	90
Sn–Mn	0.045	0.045	NaOH	1	90
Sn–Co	0.044	0.044	NaOH	5	60
Sn–Zn	0.3	0.3	NH_3 (aq.)	1	20

2. Experimental procedure

2.1 Sample preparation

All chemicals were purchased and used without further purification. Tin–metal mixed hydroxides were prepared by adding NH_3 or NaOH aqueous solutions to aqueous solutions prepared pooling together $SnCl_4·5H_2O$ and a transition metal salt ($CaSO_4·2H_2O$, $MnSO_4·H_2O$, $CoCl_2$, or $ZnCl_2$). After continuously stirring the resulting reaction solution for 1–5 h at 20–90 °C, the said solution was allowed to age for 24 h at 20 °C. As a result, precipitates formed, which were filtrated, washed with deionized water, and dried for more than 24 h at 110 °C. The reaction conditions applied for the preparation of tin–metal hydroxides are summarized in **Table 1**. The precipitates obtained from the Sn–Ca, Sn–Mn, Sn–Co, and Sn–Zn mixed solutions were named CaTO-pre, MnTO-pre, CoTO-pre, and ZnTO-pre, respectively. CaTO-pre, MnTO-pre, CoTO-pre, and ZnTO-pre were calcined at 250, 600, and 900 °C for 5 h in air to yield the corresponding Sn–metal mixed oxides, CaTO-*x*, MnTO-*x*, CoTO-*x*, and ZnTO-*x*, respectively, where *x* indicates the temperature of the final calcination process (250, 600, or 900 °C).

2.2 Characterization

X-ray diffractometry (XRD) analyses were performed using a Rigaku MiniFlexII diffractometer with Cu Kα radiation to determine the structural characteristics of the crystalline phase of the various samples. Brunauer–Emmet–Teller (BET) surface area measurements were conducted to determine both the specific surface areas and the pore diameters of samples by performing N_2 adsorption experiments at 77 K with a BEL Japan Bellsorp-mini instrument. The values of the BET specific surface area, average pore diameter, total pore volume, and mesopore volume (BJH) of the precursors before and after calcination at 250–900 °C are listed in **Table 2**. Field-emission scanning electron microscopy (FE-SEM) and transmission electron microscopy (TEM) analyses were performed on an S-5500 (HITACHI) and a JEM-2010 (JEOL) instrument, respectively. The identities and chemical states of the elements found on the sample surfaces were determined by X-ray photoelectron spectroscopy (XPS) analysis (XPS 1600E, PerkinElmer) using an Mg Kα excitation source. All the binding energy (BE) values in the XPS spectra were referenced to the C 1s line at 284.8 eV due to the presence of carbon as a contaminant. The X-ray absorption fine structure (XAFS) spectra of Sn K-edge (29.20 keV) and Zn K-edge (9.66 keV) were measured on a Spring-8 (BL01B1) instrument. The XAFS spectra of Mn K-edge (6.54 keV) and Co K-edge (7.71 keV) were measured on a Kyushu University Beamline (BL06) instrument. The powder samples utilized to conduct the XAFS measurements were pressed into pellets with a diameter of 10 mm with boron nitride powder. Notably, the XAFS measurements were carried out at room temperature in transmission mode.

Table 2. Specific surface area values and pore properties of tin–metal mixed oxide samples

Sample	S_{BET}[a] /m^2·g^{-1}	D_p[b] /nm	V_{total}[c] /cm^3·g^{-1}	V_{meso}[d] /cm^3·g^{-1}
CaTO-pre	8	5.0	0.010	0.012
CaTO-250	7	5.0	0.009	0.010
CaTO-600	5	8.0	0.010	0.011
CaTO-900	7	7.5	0.014	0.014
MnTO-pre	57	3.9	0.056	0.039
MnTO-250	112	3.7	0.104	0.080
MnTO-600	56	17.0	0.237	0.234
MnTO-900	12	6.8	0.020	0.017
CoTO-pre	9	9.1	0.021	0.020
CoTO-250	236	2.6	0.155	0.088
CoTO-600	32	11.0	0.087	0.086
CoTO-900	6	6.7	0.010	0.009
ZnTO-pre	30	3.0	0.023	0.014
ZnTO-250	101	2.6	0.065	0.035
ZnTO-600	54	4.7	0.064	0.060
ZnTO-900	5	17	0.021	0.019

a) Value for the BET specific surface area. b) Average pore diameter. c) Total pore volume. d) Mesopore volume (BJH).

3. Results and discussion

In **Figs. 1**(a)–1(d) are reported the FE-SEM images of CaTO-pre, MnTO-pre, CoTO-pre, and ZnTO-pre, respectively. As can be evinced from Fig. 1, all four precursors comprise cubic-shaped particles. The preparation conditions to obtain the cubic shape varied depending on the 'non-tin' metal. In addition, the factors controlling the size of cubic were the kind of base compound and its amount. The preparation condition of precursor for yielding the largest cubic shape of each tin–metal oxide particle in the present study are summarized in Table 1, although it is still unclear if the preparation condition of precursor is optimized. Specifically, CaTO-pre was observed to exhibit the largest particles (ca. 2 µm in length), followed by ZnTO-pre (ca. 700 nm in length). MnTO-pre and CoTO-pre samples were characterized by the smallest particles (50–200 nm in length). In Figs. 1(a')–1(d') and 1(a'')–1(d'') are reported the FE-SEM images of the corresponding tin–metal mixed oxides obtained after performing the calcinations of the precursors at 600 and 900 °C, respectively. Despite the high calcination temperature (i.e., 600 and

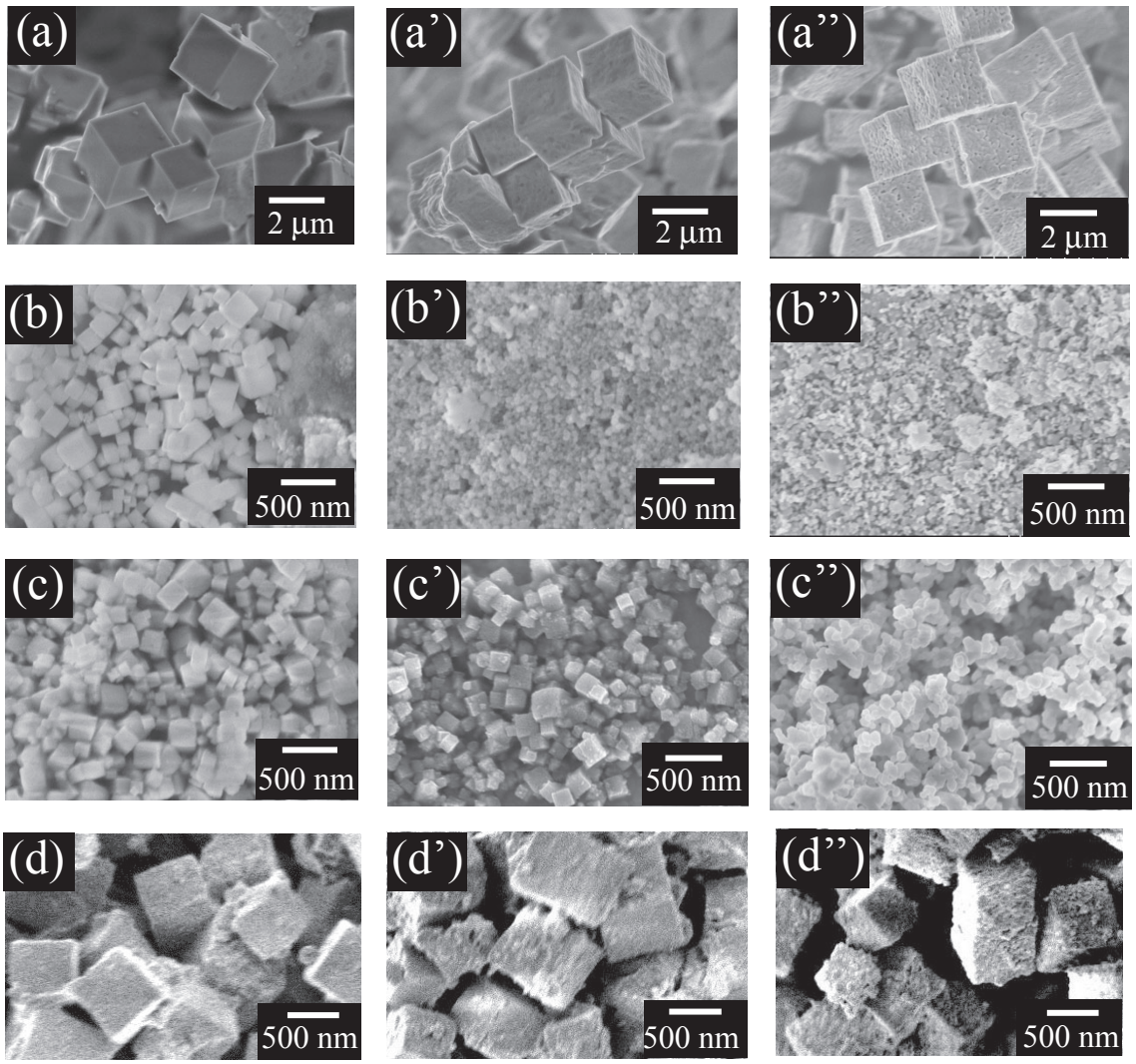

Fig. 1. Scanning electron microscopy images of (a) CaTO-pre, (a') CaTO-600, (a'') CaTO-900, (b) MnTO-pre, (b') MnTO-600, (b'') MnTO-900, (c) CoTO-pre, (c') CoTO-600, (c'') CoTO-900, (d) ZnTO-pre, (d') ZnTO-600, and (d'') ZnTO-900 samples. MTO-pre: precursor of the tin–metal mixed oxide (M: Ca, Mn, or Co); MTO-*x*: tin–metal mixed oxide obtained after precursor calcination at an *x* value for the temperature (in °C).

900 °C), CaTO-600, CaTO-900, ZnTO-600, and ZnTO-900 were observed to comprise nanoparticles of the same cubic shape and size as their respective precursors, CaTO-pre [Figs. 1(a)–1(a'')] and ZnTO-pre [Figs. 1(d)–1(d'')]. By contrast, although CoTO-600 nanoparticles exhibited the same shape as those of CoTO-pre, CoTO-900 was characterized by rounded particles, in place of cubic-shaped particles [Figs. 1(c)–1(c'')]. Finally, as a result of the calcination at 600 and 900 °C of MnTO-pre, MnTO-600 and MnTO-900 were observed to have a powdery appearance, in contrast to the cubic-shaped precursor [Figs. 1(b)–1(b'')]. Evidence thus clearly indicates that the crystal shape of tin-based precursors was dependent on the type of additive. In the present paper, the reason why CaTO-900 and ZnTO-900 retained the cubic shape even at high temperature calcination will be discussed although there were differences in particle size.

As mentioned above, both CaTO-pre and ZnTO-pre particles exhibit cubic morphologies. Based on the image reported in Fig. 1(a), the surfaces of the CaTO-pre cubic particles appear to be quite smooth. The values for the specific surface area were observed to be lower for CaTO-600 and CaTO-900 than for CaTO-pre (Table 2). This suggests that CaTO-600 was formed by maintaining high density with little pores in the cubic shape. By contrast, the specific surface area of ZnTO-600 increased to a value of 54 from that of 30 $m^2 g^{-1}$ measured for ZnTO-pre. This change may descend from the development of mesopores, as also confirmed by the data reported in Table 2. In **Figs. 2**(a) and 2(b) are reported the TEM images of ZnTO-600 and ZnTO-900, respectively. Many subnanoparticles are observed at the edge or the surface of ZnTO-600 and ZnTO-900 cubes; these subnanoparticles cause the surfaces of the cubic particles to have a rough appearance. Indeed, this roughness can also be detected in the FE-SEM images reported in Figs. 1(d') and 1(d''). The mesopore distribution in ZnTO-600 was measured performing N_2 adsorption experiments. ZnTO-600 exhibited the sharpen

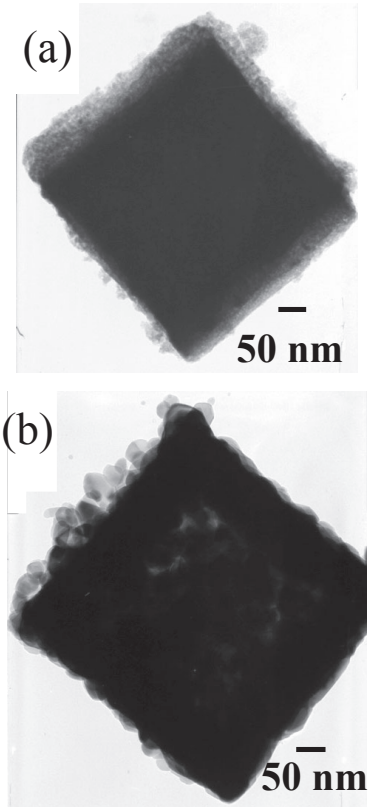

Fig. 2. TEM images of (a) ZnTO-600 and (b) ZnTO-900. ZnTO-600: tin–zinc mixed oxide obtained after precursor calcination at 600 °C. ZnTO-900: tin–zinc mixed oxide obtained after precursor calcination at 900 °C.

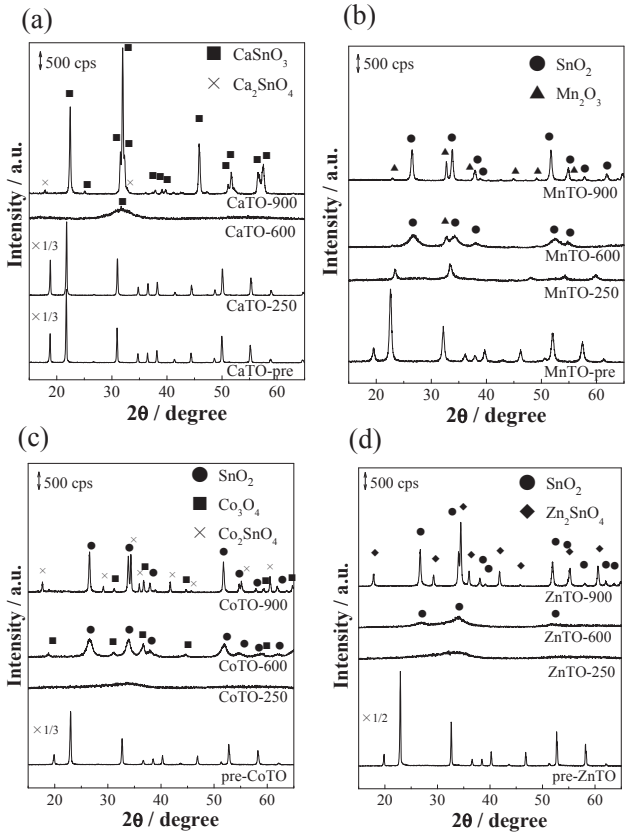

Fig. 3. X-ray diffraction patterns of (a) CaTO-*x*, (b) MnTO-*x*, (c) CoTO-*x*, and (d) ZnTO-*x* samples. MTO-*x*: tin–metal mixed oxide obtained after calcination of the precursor performed at an *x* value for the temperature (in °C).

one peak at approximately 2 nm. Based on these results, ZnTO-600 can be concluded to consist of agglomerates of nanoparticles of 50–100 nm in size, giving rise to uniform mesopores.

Except for the case of the CaTO system, precursor calcination at 250 °C was observed to result in increases in the specific surface area. By contrast, as the calcination temperature increased above 250 °C, the surface area of the MnTO, CoTO, and ZnTO systems decreased monotonously. Notably, the increase in the surface area observed as a result of calcination being performed at 250 °C is due to the increase in the number of mesopores, which are formed as a consequence of dehydration, will be discussed further when describing the results of thermogravimetry–differential thermal analysis (TG–DTA) experiments.

The crystal phase of the tin–metal mixed oxide samples was characterized by XRD (**Fig. 3**). All the diffraction peaks identified for the precursors, CaTO-pre, MnTO-pre, CoTO-pre, and ZnTO-pre, are those expected for the cubic-type lattice structure of the relevant mixed metal hydroxides: $CaSn(OH)_6$ (JCPDS No. 09-30), $MnSn(OH)_6$ (JCPDS No. 20-727), $CoSn(OH)_6$ (JCPDS No. 13-356), and $ZnSn(OH)_6$ (JCPDS No. 33-1376), respectively; no other peaks were observed.

As can be evinced from Fig. 3(a), the XRD pattern of CaTO-250 was similar to that of CaTO-pre, indicating that the crystal structure of CaTO-pre underwent no heat-induced damage during calcination performed in the temperature range between room temperature and 250 °C. In the case of the XRD pattern of CaTO-600, the peaks due to the mixed metal hydroxide were not visible, and they were replaced by a broad peak attributed to a newly formed amorphous phase. The XRD pattern of CaTO-900 included intense peaks assigned to the cubic perovskite-type oxide $CaSnO_3$ (JCPDS No. 34-939) and weak peaks due to orthorhombic Ca_2SnO_4 (JCPDS No. 46-112). Notably, the crystalline phase progressively changed with the calcination temperature, although the cubic shape of CaTO-pre nanoparticles was maintained in CaTO-600 and CaTO-900.

Similar results, such as changes in the crystal structure and no change in morphology as the calcination temperature increased, were observed in the case of ZnTO-*x*. As can be evinced from Fig. 3(d), the XRD diffraction peaks due to $ZnSn(OH)_6$ disappeared, and only a broad diffraction peak assigned to an amorphous phase was observed in the samples obtained after calcination at temperatures in the 250–600 °C range. Indeed, the XRD of ZnTO-900 exhibited new diffraction peaks with respect to the case of ZnTO-pre that were assigned to cubic Zn_2SnO_4 (JCPDS No. 73-1725) and tetragonal SnO_2 (JCPDS No. 41-1445).

When MnTO-pre and CoTO-pre were calcined at 600 °C [Figs. 3(b) and 3(c)], the XRD diffraction peaks due to the

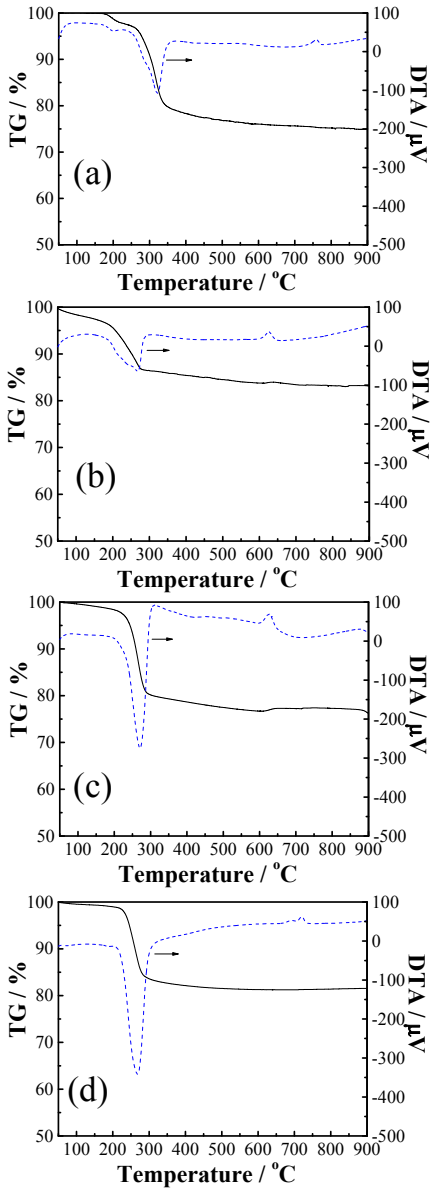

Fig. 4. Thermogravimetry (TG) and differential thermal analysis (DTA) curves for (a) CaTO-pre, (b) MnTO-pre, (c) CoTO-pre, and (d) ZnTO-pre powders. MTO-pre: precursor of the tin–metal mixed oxide (M: Ca, Mn, or Co).

relevant mixed metal hydroxides disappeared and, simultaneously, new peaks assigned to each single mixed oxide of the constituent elements, such as SnO_2, Mn_2O_3, and Co_3O_4, appeared. This indicates that the change in the crystalline phase occurs at lower temperature for MnTO-*x* and CoTO-*x* than for CaTO-*x* and ZnTO-*x*.

In **Fig. 4** are reported the TG–DTA curves obtained for CaTO-pre, MnTO-pre, CoTO-pre, and ZnTO-pre. The TG–DTA curves are essentially the same as those reported previously.[19),22)–24)] A weight loss associated with an endothermic peak was observed in the of 100–400 °C temperature range; it was assigned to the release of H_2O from $MSn(OH)_6$ (M = Ca, Mn, Co, and Zn) to yield $MSnO_3$ (or $MO + SnO_2$). The exothermic peak observed in the 600–800 °C temperature range and associated with no weight loss can be attributed to the phase transition from the amorphous to the crystallite state.[25),26)] As can be evinced from Fig. 4, the order of the crystallization temperature for the various $MSn(OH)_6$ samples is as follows: M = Ca (759 °C) > M = Zn (720 °C) > M = Mn (626 °C) ≈ M = Co (625 °C). Note that this order corresponds with the crystallinity of MTO-600 (M = Ca, Mn, Co, and Zn) samples (Fig. 3).

XPS measurements were conducted on the tin–metal mixed samples so as to investigate the chemical state of the component elements. In **Fig. 5**(A) are reported the O 1s spectra of tin–metal mixed samples. Two peaks centered at 531.0 ± 0.3 eV [peak I(O 1s)] and 530.0 ± 0.5 eV [peak II(O 1s)] were observed to overlap with each other; the peak I(O 1s) was predominantly recorded for the precursor samples; indeed, as the calcination temperature increased, the intensity of peak I(O 1s) decreased and that of peak II(O 1s) increased. Peak I(O 1s) can be attributed to the oxygen atoms of metal hydroxides whereas peak II(O 1s) can be attributed to those of metal oxides.[27)] The results reported in Fig. 5(A) are consistent with XRD data, and they indicate that the phase transition from metal hydroxide to metal oxide takes place with increasing calcination temperature.

In the Sn 3d spectra of the various tin–metal mixed samples [see Fig. 5(B)], the peaks III(Sn $3d_{5/2}$) and IV(Sn $3d_{3/2}$), which are ascribed to SnO_2,[28)] appeared at 486.5 ± 0.5 and 494.5 ± 0.5 eV, respectively. The XPS spectra in the region of Sn 3d were similar for all the samples. The Ca 2p, Mn 2p, Co 2p, and Zn 2p XPS spectra of the tin–metal mixed samples are reported in Fig. 5(C). The BEs of Ca $2p_{3/2}$ and Zn $2p_{3/2}$ in the various calcination temperature were 346.5 ± 0.3 and 1021.0 ± 0.3 eV, respectively, which are attributable to Ca(II) and Zn(II) in CaO and ZnO, respectively.[29),30)] The Co $2p_{3/2}$ peak was observed at 781.1 eV for CoTO-pre, and it exhibited a satellite peak (at ca. 787 eV), which is characteristic of Co(II). When CoTO-pre was calcined at 600 °C to produce CoTO-600, the position of the peak due to Co(II) (Co $2p_{3/2}$) shifted to lower BE values (by ca. −1.0 eV), and the satellite peak decreased in intensity. This observation indicates that Co(II) determined to be present in CoTO-pre and CoTO-250 was oxidized to Co(III) as a result of calcination process conducted at 600 °C.[31)] A similar observation was made in the case of MnTO-*x*. The BE of Mn $2p_{3/2}$ of MnTO-pre was observed at 641.8 eV, and its position shifted to 642.7 eV (+0.9 eV) after calcination process was performed at 600 °C to produce MTO-600. Similarly to the case of the tin–cobalt mixed species, this result suggests that the Mn(II) present in MnTO-pre was oxidized to Mn(III) as a result of calcination.[29)]

Based on the results of the XRD, TG–DTA, and XPS experiments, the following conclusions on the calcination process of tin–metal mixed hydroxides to produce tin–metal mixed oxides can be made: (1) the crystalline phase of tin–metal mixed hydroxides was transformed into an amorphous phase once by calcination, a process accom-

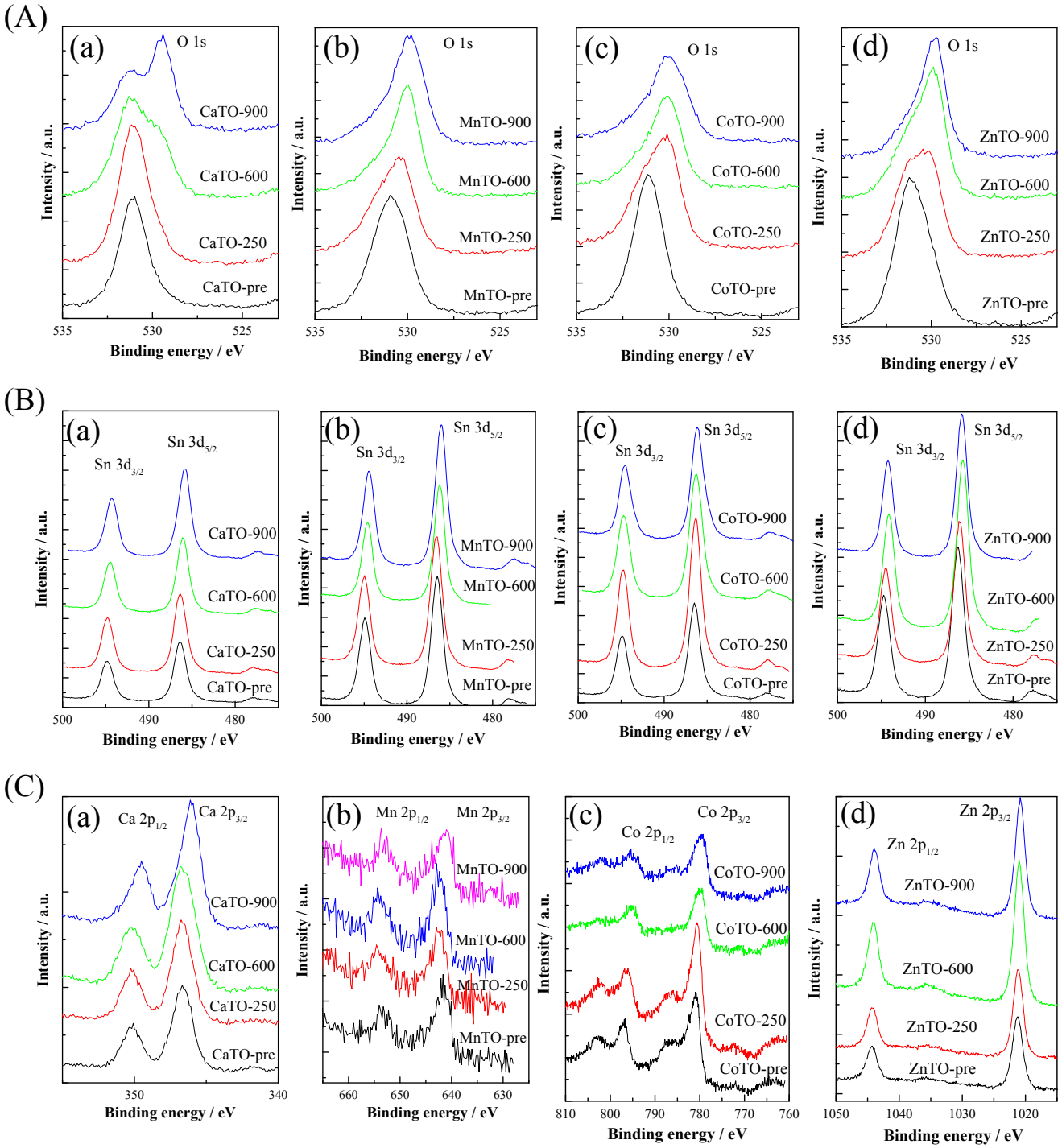

Fig. 5. (A) O 1s, (B) Sn 3d, and (C) additive 2p X-ray photoelectron spectra of (a) CaTO-*x*, (b) MnTO-*x*, (c) CoTO-*x*, and (d) ZnTO-*x*. MTO-*x*: tin–metal mixed oxide obtained after calcination of the precursor performed at an *x* value for the temperature (in °C; M: Ca, Mn, Co, or Zn).

panied by the desorption of water (as indicated by XRD and TG–DTA data); (2) at the calcination temperatures above 600 °C, a new crystalline phase assigned to tin–metal mixed oxide was observed by XRD, TG–DTA, and XPS; (3) Co(II) in CoTO-pre and Mn(II) in MnTO-pre underwent oxidization to Co(III) and Mn(III), respectively, as a result of calcination conducted at temperatures higher than 600 °C.

XAFS is a powerful tool to gather information on the local structure of compounds. Therefore, we performed XAFS experiments on tin–metal mixed compounds with the goal of investigating the structures of small crystallites or amorphous particles, which cannot be detected by XRD. **Figures 6**(a)–6(c) show the Mn-K, Co-K, and Zn-K edge X-ray absorption near edge structure (XANES) spectra of MnTO-*x*, CoTO-*x*, and ZnTO-*x*, respectively. XANES

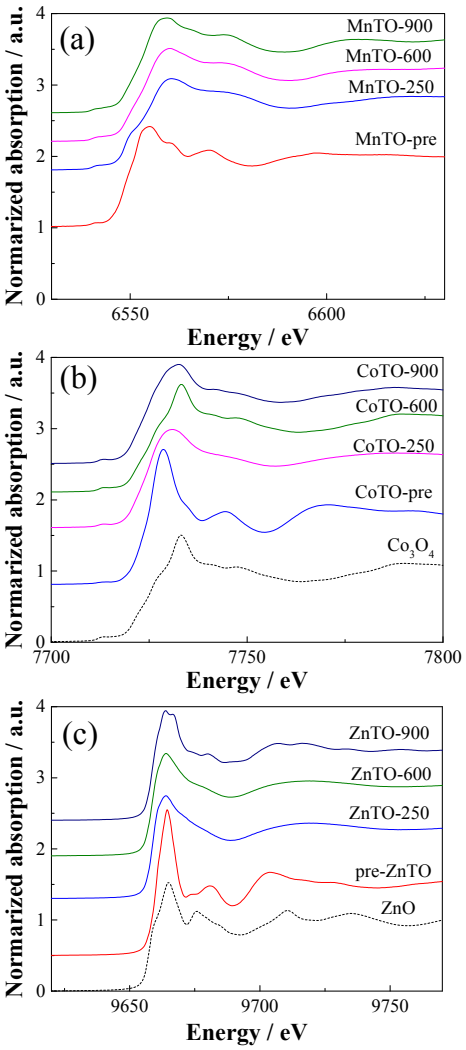

Fig. 6. (a) Mn-K, (b) Co-K, and (c) Zn-K edges XANES spectra of MTO-*x* samples. MTO-*x*: tin–metal mixed oxide obtained after calcination of the precursor performed at an *x* value for the temperature (in °C; M: Mn, Co or Zn).

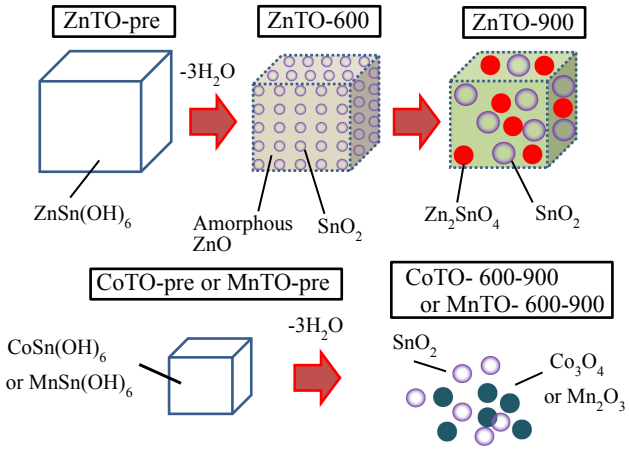

Fig. 7. Schematic representation of the proposed calcination process.

spectra of CaTO-*x* could not be analyzed because of the overlapping of Ca K-edge (4038 eV), Sn L3-edge (3929 eV), and Sn L2-edge (4156 eV). As can be evinced from the spectra depicted in Fig. 6(a), the shape of the adsorption edge of the XANES spectrum of MnTO-pre was in an agreement with that of Mn(II), and the shapes of the adsorption edges of the XANES spectra of MnTO-600 and MnTO-900 were in agreement with that of Mn(III).[33] The formation of Mn_2O_3 [Mn(III)] is consistent with XRD and XPS results [see Figs. 3(b) and 5(C)]. A similar oxidation was determined to occur as a result of the calcination process, based on the XANES spectra of the CoTO-*x* samples. As can be evinced from Fig. 6(b), the Co-K XANES spectrum of CoTO-pre was different from that of CoTO-600, suggesting that the calcination process at 600 °C had resulted in the oxidation of Co(II) to Co(III).[34]

On the other hand, the Zn-K edge XANES spectrum of ZnTO-pre in Fig. 6(c) was observed to be different from those of ZnTO-250, ZnTO-400, ZnTO-600, and ZnO, indicating the different electronic state of the Zn ion in ZnTO-pre, with respect to all the other species. Furthermore, the Zn-K edge XANES spectra of ZnTO-250, ZnTO-400, and ZnTO-600 comprised a broader peak than the corresponding spectrum of ZTO-pre. This observation implies that multiple Zn–O coordination states exist, like amorphous for ZnTO-250, ZnTO-400, and ZnTO-600. A similar result was reported by Hoel et al.;[32] in fact, these researchers assigned XAFS spectrum to ZnO amorphous phase in Zn–Sn–In oxide. Accordingly, the electronic state of Zn was not changed above 250 °C, which led to the maintenance of the cubic shape.

On the basis of the abovementioned experimental results, a plausible model was proposed for the calcination of the Sn–Zn precursor to yield the Sn–Zn mixed oxide (see **Fig. 7**). Specifically, a uniform $ZnSn(OH)_6$ precursor (ZnTO-pre) is initially prepared implementing the coprecipitation method detailed above. At 600 °C of calcination temperature, ZnTO-pre undergoes dehydration, and simultaneously, subnanosized particles are formed that consist of SnO_2 and amorphous ZnO. A further increase in the calcination temperature to 900 °C results in the growth of SnO_2 crystals and the formation of Zn_2SnO_4, although cubic shapes are maintained in these calcination processes. In the range from 700 to 900 °C of calcination temperature, the XRD peak intensities of Zn_2SnO_4 and SnO_2 increased with increasing calcination temperature, indicating the increment of the crystallite size.[1] This result suggests that Zn_2SnO_4 and SnO_2 subnanosized particles grow up to bulk. The reason that, in contrast to the cases just described, the cubic shape of the nanoparticles that make up the MnTO and CoTO samples was not maintained after calcination may have to do with the structural rearrangement necessary when the O-binding Mn and Co ions undergo valence change as part of the calcination process. Several crystal phases, such as perovskite ($CaSnO_3$) and spinels (Ca_2SnO_4, Co_2SnO_4, and Zn_2SnO_4), were observed in MTO-900 samples, the type of crystal phase being different depending on the non-tin metal. The plausible reason is as follows. In the cases of MnTO-*x* and CoTO-*x*

samples, the structure destabilization occurs due to the change in valence at calcination temperature as low as 600 °C and the different crystal phases, such as SnO_2, Mn_2O_3, and Co_3O_4, are simultaneously formed. As a result, the crystal growth of the spinels (Mn_2SnO_4 and Co_2SnO_4) may be difficult to occur. In contrast, in the case of CaTO-*x*, the CaTO-pre structure is more stable and maintains its structure up to around 600 °C. Therefore, the formation of complex oxides ($CaSnO_3$ and Ca_2SnO_4) is assumed to be facilitated than the formation of SnO_2. Further studies concerning oxide formation are necessary.

4. Conclusions

We focused on the transformation of cubic-shaped tin–metal mixed hydroxides to tin–metal mixed oxides by heat treatment. Indeed, four tin–metal mixed hydroxides, $CaSn(OH)_6$, $MnSn(OH)_6$, $CoSn(OH)_6$, and $ZnSn(OH)_6$, with cubic morphology were prepared by a coprecipitation method. The size of cubic-shaped mixed hydroxide nanoparticles decreased in the following order: $CaSn(OH)_6$ (ca. 2 μm) > $ZnSn(OH)_6$ (ca. 700 nm) > $MnSn(OH)_6 \approx CoSn(OH)_6$ (50–200 nm). The tin–metal mixed hydroxides were then transformed to the corresponding oxides by calcination conducted at 600–900 °C. By this approach, cubic perovskite-type $CaSnO_3$ and orthorhombic Ca_2SnO_4 were obtained from $CaSn(OH)_6$, cubic Zn_2SnO_4 and tetragonal SnO_2 were obtained from $ZnSn(OH)_6$, SnO_2 and Mn_2O_3 were obtained from $MnSn(OH)_6$, and SnO_2 and Co_3O_4 were obtained from $CoSn(OH)_6$. This indicated that by calcining $CaSn(OH)_6$ and $ZnSn(OH)_6$ at 600 and 900 °C, mixed oxides were obtained that, much like their hydroxide precursors, comprised cubically shaped nanoparticles; by contrast, the cubic shape of $MnSn(OH)_6$ and $CoSn(OH)_6$ nanoparticles was not maintained when a similar heat treatment was applied to obtain the corresponding mixed oxides. XAFS result suggested that such a cubic shape is stabilized in the thermal treatment of $ZnSn(OH)_6$. In addition, the change in valence of the metal ions present in the Co-containing and Mn-containing mixed oxides with respect to their counterparts present in the precursors destabilizes the cubic shape of the nanoparticles.

References

1) S. Yamaguchi, H. Yamaura, K. Morihara, M. Iwasaki and H. Yahiro, *Chem. Lett.*, 45, 851–853 (2016).
2) C. Wang, X. Wang, J. Zhao, B. Mai, G. Sheng, P. Peng and J. Fu, *J. Mater. Sci.*, 37, 2989–2996 (2002).
3) W. W. Wang, Y. J. Zhu and L. X. Yang, *Adv. Funct. Mater.*, 17, 59–64 (2007).
4) J. Zeng, M. D. Xin, K. W. Li, H. Wang, H. Yan and W. J. Zhang, *J. Phys. Chem. C*, 112, 4159–4167 (2008).
5) J. H. Yu and G. M. Choi, *Sensor. Actuat. B-Chem.*, 52, 251–256 (1998).
6) J. H. Yu and G. M. Choi, *Sensor. Actuat. B-Chem.*, 72, 141–148 (2001).
7) J. H. Ko, I. H. Kim, D. Kim, K. S. Lee, T. S. Lee, B. Cheong and W. M. Kim, *Appl. Surf. Sci.*, 253, 7398–7403 (2007).
8) Z. Yuan, F. Huang, J. Sun and Y. Zhou, *Chem. Lett.*, 31, 408–409 (2002).
9) T. L. Villarreal, G. Boschloo and A. Hagfeldt, *J. Phys. Chem. C*, 111, 5549–5556 (2007).
10) X. Ding, D. Zeng and C. Xie, *Sensor. Actuat. B-Chem.*, 149, 336–344 (2010).
11) X. Y. Xue, T. L. Guo, Z. X. Lin and T. H. Wang, *Mater. Lett.*, 62, 1356–1358 (2008).
12) B. Geng, C. Fang, F. Zhan and N. Yu, *Small*, 4, 1337–1343 (2008).
13) W. Wang, Z. Ma, R. Liang, T. Wu and Y. Wu, *J. Mater. Res.*, 28, 1582–1588 (2013).
14) J. Huang, X. Xu, C. Gu, W. Wang, B. Geng, Y. Sun and J. Liu, *Sensor. Actuat. B-Chem.*, 171–172, 572–579 (2012).
15) Z. Wang, J. Liu, F. Wang, S. Chen, H. Luo and X. Yu, *J. Phys. Chem. C*, 114, 13577–13582 (2010).
16) J. H. Lee, *Sensor. Actuat. B-Chem.*, 140, 319–336 (2009).
17) G. Ma, R. Zou, L. Jiang, Z. Zhang, Y. Xue, L. Yu, G. Song, W. Li and J. Hu, *CrystEngComm*, 14, 2172–2179 (2012).
18) Y. Cao, D. Jia, J. Zhou and Y. Sun, *Eur. J. Inorg. Chem.*, 2009, 4105–4109 (2009).
19) J. Huang, X. Xu, C. Gu, W. Wang, B. Geng, Y. Sun and J. Liu, *Sensor. Actuat. B-Chem.*, 173, 599–606 (2012).
20) J. Huang, L. Wang, C. Gu and J. J. Shim, *Mater. Lett.*, 136, 371–374 (2014).
21) P. Cheng, Y. Ni, K. Yuan and J. Hong, *Mater. Lett.*, 90, 19–22 (2013).
22) T. Liu, R. Du, X. Kong and J. Wang, *J. Chem. Pharm. Res.*, 6, 1490–1495 (2014).
23) S. Lei, K. Tang, C. Chen, Y. Jin and L. Zhou, *Mater. Res. Bull.*, 44, 393–397 (2009).
24) W. Tang, J. Wang, P. Yao and X. Li, *J. Mater. Sci.*, 49, 1246–1255 (2014).
25) F. Huang, X. Z. Lu, Y. Liu, J. Liu and R. Wu, *Mater. Sci. Tech.-Lond.*, 27, 29–34 (2011).
26) Q. He, J. Zi, B. Huang, L. Yan, W. Fa, D. Li, Y. Zhang, Y. Gao and Z. Zheng, *J. Alloy. Compd.*, 607, 193–197 (2014).
27) H. B. Yao, Y. Li and A. T. S. Wee, *Appl. Surf. Sci.*, 158, 112–119 (2000).
28) J. Long, W. Xue, X. Xie, Q. Gu, Y. Zhou, Y. Chi, W. Chen, Z. Ding and X. Wang, *Catal. Commun.*, 16, 215–219 (2011).
29) Y. Liu, T. Gu, Y. Wang, X. Weng and Z. Wu, *Catal. Commun.*, 18, 106–109 (2012).
30) R. K. Sahu, K. Ganguly, T. Mishra, M. Mishra, R. S. Ningthoujam, S. K. Roy and L. C. Pathak, *J. Colloid Interf. Sci.*, 366, 8–15 (2012).
31) S. C. Petitto, E. M. Marsh, G. A. Carson and M. A. Langell, *J. Mol. Catal. A-Chem.*, 281, 49–58 (2008).
32) C. A. Hoel, S. Xie, C. Benmore, C. D. Malliakas, J. F. Gaillard and K. R. Poeppelmeier, *Z. Anorg. Allg. Chem.*, 637, 885–894 (2011).
33) H. Einaga, S. Yamamoto, N. Maeda and Y. Teraoka, *Catal. Today*, 242, 287–293 (2015).
34) M. Nishibori, W. Shin, N. Izu, T. Itoh and I. Matsubara, *Catal. Today*, 201, 85–91 (2013).